Quantitative Assessment of Lung Using Hyperpolarized Magnetic Resonance Imaging

Kiarash Emami[1], Michael Stephen[2], Stephen Kadlecek[1], Robert V. Cadman[1], Masaru Ishii[3], and Rahim R. Rizi[1]

[1]Department of Radiology, and [2]Pulmonary, Allergy, and Critical Care Division, University of Pennsylvania, Philadelphia, Pennsylvania; and [3]Department of Otolaryngology, Johns Hopkins University, Baltimore, Maryland

Improvements in the quantitative assessment of structure, function, and metabolic activity in the lung, combined with improvements in the spatial resolution of those assessments, enhance the diagnosis and evaluation of pulmonary disorders. Radiologic methods are among the most attractive techniques for the comprehensive assessment of the lung, as they allow quantitative assessment of this organ through measurements of a number of structural, functional, and metabolic parameters. Hyperpolarized nuclei magnetic resonance imaging (MRI) has opened up new territories for the quantitative assessment of lung function and structure with an unprecedented spatial resolution and sensitivity. This review article presents a survey of recent developments in the field of pulmonary imaging using hyperpolarized nuclei MRI for quantitative imaging of different aspects of the lung, as well as preclinical applications of these techniques to diagnose and evaluate specific pulmonary diseases. After presenting a brief overview of various hyperpolarization techniques, this survey divides the research activities of the field into four broad areas: lung microstructure, ventilation, oxygenation, and perfusion. Finally, it discusses the challenges currently faced by researchers in this field to translate this rich body of methodology into wider-scale clinical applications.

Keywords: hyperpolarized gas MRI; hyperpolarized ^{13}C MRI; quantitative lung imaging

Improvements in the quantitative assessments of structure, function, and metabolic activity in the lung, combined with improvements in the spatial resolution of those assessments, enhance the diagnosis and evaluation of pulmonary disorders. Radiologic methods are among the most appealing techniques, as they allow for comprehensive quantitative assessment of the lung through measurements of a number of structural, functional, and metabolic parameters. In addition, these radiologic methods are rapid, easily applied, reproducible, safe when performed infrequently, and tolerable by patients with advanced pulmonary disorders. The chief methods for assessing the distribution of the ventilation to perfusion ratio ($\dot{V}_A/\dot{Q}$) are ^{133}Xe and ^{99m}Tc-labeled macro-aggregated albumin (1). However, conventional $\dot{V}_A/\dot{Q}$ nuclear scanning has limited spatial resolution and requires exposure to radioactive agents. In recent years, quantitative multi-detector computed tomography (MDCT) imaging has also generated considerable enthusiasm and impressive clinical utility for staging and phenotyping many lung diseases, especially emphysema (2). Use of this technology has been limited due to safety issues in regards to the ionizing radiation that prevents the repetition of tests at a frequency sufficient for both disease management and the assessment of therapeutic interventions. A third approach, proton magnetic resonance imaging (MRI), suffers from low signal intensity caused by low tissue density, resulting in poor image quality. However, several new developments have allowed for improved proton imaging of lung parenchyma, specifically the recent development of more efficient pulse sequences with very short echo times (3). Some attempts have been made to use conventional MRI techniques for the functional assessment of the lung. One such approach has been the use of the arterial spin-tagging (AST) method of perfusion imaging, which has been implemented successfully in both animal and human studies (4). Several researchers have also used oxygen-enhanced MRI as a measure of ventilation (5). While these proton-based MRI techniques have made functional MRI of pulmonary ventilation and perfusion possible, acquiring high-resolution structural and functional images of the actual lung air spaces with these methods remains a difficult task.

The introduction of hyperpolarized (HP) nuclei into medical research promises to transform MRI from a modality with little utility in lung imaging to one that can be used to measure pulmonary structure, function, and metabolism with high resolution and sensitivity. This technology permits an agent to be prepared external to the MRI scanner so that, upon administration to the subject within the scanner, the MRI signal from the agent is enhanced by several orders of magnitude. This is most efficiently done through the use of three methods of hyperpolarization: optical pumping, dynamic nuclear polarization, and para-hydrogen induced polarization. As is typical of MR-based measurements, MRI pulse sequences for HP nuclei can be tailored to improve sensitivity in specific features of the lung.

In what follows, we briefly describe the current state and recent advancements in the field of hyperpolarized MRI for the quantitative imaging of the lung.

This review will cover innovative techniques developed to use hyperpolarized gas (HPG) and ^{13}C MRI technologies for lung assessment, as well as pre-clinical applications of these techniques to diagnose and evaluate specific pulmonary diseases. After presenting an overview of various hyperpolarization techniques, this survey divides the research activities of the field into the following broad areas: lung microstructure, ventilation, oxygenation, and perfusion.

PRODUCTION OF HYPERPOLARIZED NUCLEI

The optical pumping methods used for hyperpolarizing ^{3}He and ^{129}Xe noble gases to enhance their achievable MR signal-to-noise ratio fall into two broad categories: spin exchange optical pumping (SEOP) and metastability exchange optical pumping (MEOP) (6, 7). These technologies offer an opportunity to combine the flexibility and safety of MRI with the large signal-to-noise ratio obtainable through the use of hyperpolarization. One established application of this technology is pulmonary imaging, where a series of polarized gas MR images are obtained upon inhalation of these gases. It is then possible to extract from the images a number of structural and physiologic parameters for the quantitative assessment of lungs, including

(*Received in original form February 23, 2009; accepted in final form June 23, 2009*)

Supported by grants NIH R01-HL064741 and R01-HL077241.

Correspondence and requests for reprints should be addressed to Rahim R. Rizi, Ph.D., Associate Professor of Radiology, University of Pennsylvania, Department of Radiology, 1 Silverstein Bldg., 3400 Spruce Street, Philadelphia, PA 19104. E-mail: rizi@uphs.upenn.edu

Proc Am Thorac Soc Vol 6. pp 431–438, 2009
DOI: 10.1513/pats.200902-008AW
Internet address: www.atsjournals.org

the apparent diffusion coefficient (ADC), regional ventilation, regional partial pressure of oxygen, and the oxygen depletion rate.

Similarly, dynamic nuclear polarization (DNP) and parahydrogen–induced polarization (PHIP) have shown a potential to produce large quantities of highly polarized compounds that could potentially be used for functional, structural, and metabolic assessment of the lung. While optical techniques have been used mostly to hyperpolarize noble gases, these two other technologies have been commonly used to hyperpolarize ^{13}C and ^{15}N nuclei (11, 12).

ASSESSMENT OF LUNG MICROSTRUCTURE

The ^{3}He atoms in a gas undergo a Brownian random motion. The average traveled distance of the gas atoms during a given duration of time is determined by the diffusion coefficient D, specific to the gas or gas mixture. The measured value of D is termed the apparent diffusion coefficient (ADC). Under standard temperature and pressure conditions (20°C and 101.325 kP absolute), and without restricting barriers, D is 2.05 cm^2/second in pure ^{3}He gas (8) and approximately 0.88 cm^2/second for ^{3}He diluted in atmospheric gases (9). If gas diffusion in the lung is measured, however, the diffusion coefficient is much smaller and is not homogeneous. The bulk of this difference and heterogeneity indicates diffusion hindrance by the lung structure itself. ADC measurements are therefore altered by changes in the lung microstructure. ADC appears to be a sensitive (10) and reproducible (11) marker for the early detection (12) and analysis of progression (13) of diseases and other processes affecting the size of alveoli and small airways (9).

Using even a very fast MRI acquisition time of 1 millisecond, a free ^{3}He atom will move a substantial fraction of 1 mm during the measurement. Since the healthy human alveolar radius is 135 to 250 μm (and this does not vary significantly for other mammals), the motion of the ^{3}He atoms is severely restricted by lung structure. In contrast, the motion of the ^{3}He atoms is less restricted in diseased lungs due to the large alveolar size. Chen and coworkers (8) reported the first *in vivo* measurements of lung geometric parameters at the alveolar level obtained with ^{3}He diffusion MRI. Further studies in animals (14, 15), healthy human subjects, and patients with severe emphysema (10) have clearly shown substantial differences in ADC values between healthy and emphysematous lungs at the acinar level. Using a more sophisticated model, Yablonskiy and colleagues (9) have reported significant anisotropy in the apparent diffusion coefficient due to the directional nature of the pulmonary tree, and have published a ^{3}He lung diffusion model that relates the alveolar geometrical parameters to the apparent diffusion coefficient.

Much of work in the area of HPG diffusion MRI has focused on the short-range ADC measurements over a few milliseconds (16), which is sensitive to morphology at the alveolar level. In contrast, the long-time-scale ADC measurement by which diffusion is observed over the period of approximately 1 second, helium atoms can travel over distances that are much greater than the characteristic dimensions of the alveoli, and consequently are expected to also reflect the connectivity of the small airspaces of the lung (17). An emerging interest in recent years has been the development and use of techniques for long-range ADC measurements, since these may exhibit different sensitivity to various lung diseases. Wang and coworkers developed and implemented a technique for measurement of long-time-scale ADC of hyperpolarized gases (18), and tested it in 10 healthy subjects and in 2 subjects with chronic obstructive pulmonary disease (COPD) with a range of diffusion times from a few tenths of a second to several seconds. Figure 1 shows short- and long-range ADC maps of a representative healthy subject and a subject with COPD. Results showed that for the two subjects with COPD, long-range ADC values (expressed in cm^2/s) were substantially greater than those of healthy subjects at all diffusion times: 0.08 ± 0.08 cm^2/second versus 0.04 ± 0.01. The short-range ADC values were respectively measured at 0.31 ± 0.41 versus 0.23 ± 0.05. These findings therefore suggest that the long-time-scale diffusion measurements can be more sensitive than their short-time counterparts for detecting emphysematous changes in the lungs.

Currently no measurement technique directly comparable to ADC exists, so its potential clinical applications are various and readily influenced by unique ideas. The closest surrogate is the measurement of lung tissue destruction on CT scans through Hounsfield unit analysis. The detection of lung tissue destruction by CT, specifically in the upper lobes, has found an important clinical niche in stratifying which patients with COPD will benefit from lung volume reduction surgery (19). There is hope that ADC will be capable of finding a similar clinical role. It currently is being investigated as a predictor of disease progression in patients with COPD, and hopefully will be able

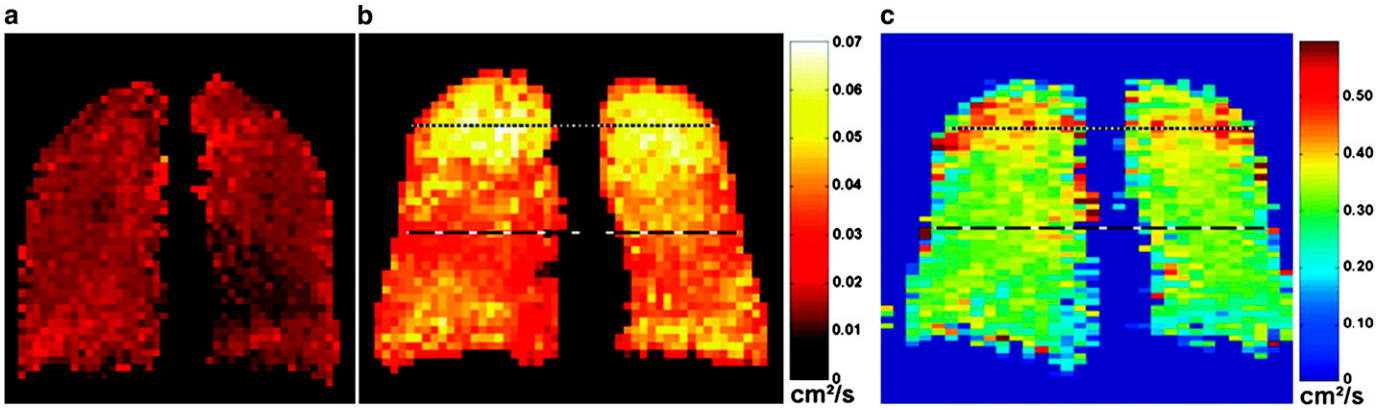

Figure 1. Coronal projection long-time-scale apparent diffusion coefficient (ADC) maps from (*a*) a healthy subject and (*b*) a subject with subclinical chronic obstructive pulmonary disease (COPD). In *b,* markedly elevated ADC values are present in the lung apices, and moderately elevated ADC values are present in the mid-section of the lung. (*c*) Coronal projection short-time-scale ADC map from the same subject with subclinical COPD. Mildly elevated ADC values are present in the apices. Reprinted by permission from Reference 18.

to stratify patients so that the natural history of a patient's disease can be better predicted. Currently there is little idea as to which smokers will develop life-threatening emphysema, and a majority in fact do not. Recent clinical trials of pharmaceuticals are therefore using a very heterogeneous population and thus to date there is no available medication that has been shown to slow the progression of disease (20). If ADC could demonstrate that occult destruction is a predictor of future outcomes, this would greatly support the encouragement to quit tobacco, as well as allowing for the testing of potentially life-saving medications in a more homogenous and suitable population. Besides acting as a predictor, ADC could be used as a clinical endpoint of change in COPD and other airways in clinical disease trials, as it is quantifiable and can be done without the risk of radiation. Beyond COPD, ADC has implications in the treatment of asthma as the disease progresses from reversibility to irreversibility, as well as in the management of interstitial lung diseases, acting as a surrogate for alveolar thickness information. Whether it could also be used for diagnosing conditions like small airways disease is unclear, but it remains another important potential application.

Several small-scale studies have been performed to address the validity of ADC measurements in the lung. In the absence of adequate imaging or a gold standard for tissue remodeling, the studies have either focused on correlations between surrogate measures (e.g., FEV_1 and CT X-ray opacity) and ADC or compared ADC to metrics derived from histologic sections. The most extensive studies in human subjects appear in the article by Diaz and colleagues (21), and show a highly significant correlation between the mean ^{3}He ADC measurement and two CT-derived metrics (mean lung density [MLD] and the 15th percentile Hounsfield unit cutoff), as well as between ^{3}He ADC and the PFT-derived diffusing capacity for carbon monoxide (D_{LCO}), with $P < 0.01$ in each case. The correlation between D_{LCO} and mean ^{3}He ADC was found to be much more significant than between D_{LCO} and either of the CT indices ($r = -0.82$, $P < 10^{-4}$ as compared with $r = 0.60$ and $r = 0.29$ for D_{LCO}/15th percentile and D_{LCO}/MLD). The highest correlation was seen between ^{3}He mean ADC and CT 15th percentile cutoff ($r = -0.90$, $P < 10^{-5}$), suggesting that ADC measurements are sensitive to the same loss of tissue density that is measured using CT but, given the stronger relationship with D_{LCO}, are more specific to changes in tissue density that result in impaired gas exchange.

A recent study has directly addressed the sensitivity of ^{3}He ADC–derived measurements to early stages of disease. In an imaging trial of eleven asymptomatic smokers and eight healthy control subjects by Fain and coworkers (12), a significant correlation was found between pack-years of smoking and whole-lung mean ADC ($r = 0.60$, $P = 0.007$). No correlation was found between a commonly used CT-derived index (RA_{950}, or the fraction of lung volume with < -950 HU attenuation) and pack-years of smoking, indicating that at least one ^{3}He-based metric is better able to discriminate changes to the lung associated with early stages of disease.

Attempting to directly compare regional ADC measurements to histology, Woods and colleagues used specimens (1.3 cm diameter $\times$ 2 cm thick) from transplanted human lungs and showed an inverse correlation between diffusivity and surface area to volume ratio (SA/V) and a positive correlation between diffusivity and mean linear intercept (Lm) (22). This work concluded that ^{3}He ADC measurements separated normal from emphysematous lung tissue with better accuracy than the morphometric analyses. In the most recent validation study, Jacob and coworkers (23) investigated the regional correlation of ADC measurements and quantitative histology in rat lungs. This study showed that the average ^{3}He ADC correlates well with histology ($r = 0.85$, $P < 10^{-4}$), thereby concluding that ^{3}He ADC is a viable noninvasive morphometric tool for the localized *in vivo* assessment of emphysema.

ASSESSMENT OF LUNG FUNCTION

Measurement of Pulmonary Oxygen Tension with Hyperpolarized Gases

Most of the hyperpolarized gas functional lung measurements in common use rely on, or require correction for, the interaction of HPG and oxygen in the gas phase. Hyperpolarized gas gradually loses its polarization in the presence of oxygen due to molecular dipole interactions between the two species. The rate at which this depolarization occurs depends on the molecular collision rate and therefore on the relative concentration in the gas mixture. Saam and colleagues (24) found a linear relationship for ^{3}He gas between the oxygen-induced decay time constant and the alveolar oxygen partial pressure: $T_{1,O_2} = \xi / P_A O_2$, with a proportionality constant of $\xi = 2.6$ bar $\cdot$ s at body temperature.

A number of investigators have explicitly measured the effect of O_2-induced depolarization to yield another set of functional lung measurements. If one can measure the gas relaxation rate and its time derivative with sufficient accuracy, then the alveolar partial pressure of oxygen ($P_{A_{O_2}}$) and rate of oxygen uptake into the bloodstream (the O_2 depletion rate, or ODR) can be determined from a series of hyperpolarized ^{3}He images. Details on how such images can be converted into partial pressures of oxygen and oxygen uptake rate are given elsewhere (25). These techniques require a series of images with at least two different inter-image delays to make use of the differing dependencies on delay time. Published techniques differ in the number of breath-holds required for the subject and the overall accuracy and sensitivity when dealing with an incomplete breath-hold, as short as 15 seconds (26–28). Breath-hold requirements in this procedure may be difficult for severely diseased patients, since an accurate measurement requires inter-image delays on the order of the characteristic oxygen-induced relaxation time, which is several seconds at physiologic O_2 concentrations.

The fundamental approach for performing measurements of pulmonary oxygen tension has remained unchanged for the past few years. However, an important new development in this area is the recently developed technique for the simultaneous measurement of $P_{A_{O_2}}$, ODR, and ADC in one single breath-hold (29). This technique is of practical significance in human subjects, as it allows for the acquisition of spatially correlated measurements of lung oxygen tension and gas diffusion. Moreover, performing both measurements in one breath-hold decreases both the scan time and the required amount of HPG. Figure 2 shows the application of this technique in a 52-year-old female patient with severe COPD during a 26-second breath-hold. The images correspond to a 50-mm coronal middle slice and indicate a poorly ventilated region in the upper right lobe. It is also interesting to note the compromised ODR (2.0 mm Hg/s) in the same region exhibiting high ADC values ($\sim$0.85 cm^2/s), indicating the correlated changes of lung function and structure in obstructive lung diseases. The same group of researchers reported another study for *in vivo* reproducibility measurements of $P_{A_{O_2}}$ and ODR (30) in pigs, and showed that the average variation of mean is 11% for $P_{A_{O_2}}$ and 24% for ODR. Finally, Patz and colleagues recently demonstrated for the first time an implementation of $P_{A_{O_2}}$ measurements based on HP ^{129}Xe MRI in human subjects (31).

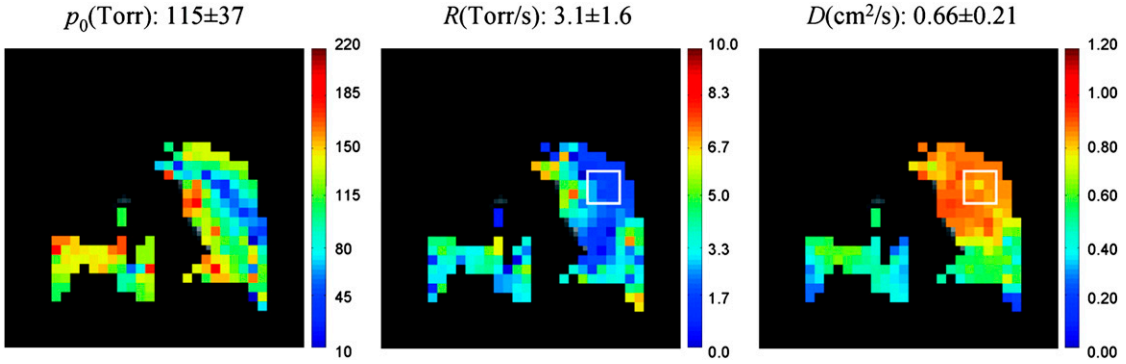

Figure 2. Simultaneous measurement of $P_{A_{O_2}}$, O_2 depletion rate (ODR), and ADC with HP ^{3}He MRI in a patient with COPD. In the selected region, ADC value is 29% higher while ODR value is 61% lower than the corresponding global average values. This correlated change can be representative of the lung tissue destruction with gas exchange deficiency. The missing lobe on the upper portion of the right lung is indicative of a substantial ventilation defect. Reprinted by permission from Reference 29.

The direct measurement of regional alveolar oxygen tension is a completely novel metric. Clinicians have traditionally guessed at the lung oxygen tensions based on an estimate of inspired gas concentration and a presumed minute ventilation. This quantity has never been measured directly, but its assessment could have wide-ranging implications for the investigation of ventilation and its impact on regional oxygen concentrations. Ventilation is thought to increase from apices to bases based on nuclear scintigraphy studies. From this, estimations of oxygen tensions have been proposed for a $P_{A_{O_2}}$ of 130 mm Hg at the apex to 90 mm Hg at the base (32). This gradient is believed to switch horizontally when a patient changes from an upright to a supine position. The measurement of $P_{A_{O_2}}$ could help confirm these ventilation studies, while investigating new areas of gas distribution pathology. One specific area where this could be employed is in the detection of acute pulmonary embolus, where there may be needed a more sensitive technique than simple ventilation to pick up an airway lesion associated with the inflammation of a pulmonary embolus. Another area of investigation would be in critically ill patients, where there are issues of oxygen toxicity. Assessing how different oxygen tensions throughout the lung may help or harm a patient during their hospital stay would be a novel area of research.

Although oxygen tension imaging techniques are less well tested than the other ^{3}He MRI–based measurements, preliminary results demonstrate the repeatability and physiologic plausibility of $P_{A_{O_2}}$ measurements in animal and human subjects. The absence of a direct *in vivo* measurement technique for regional alveolar oxygen concentration has limited the validation to phantoms (33). Direct comparison to radionuclide scans or invasive $P_{A_{O_2}}$ measurements, however, are among potential approaches in evaluating the accuracy and precision of a ^{3}He MRI–based oxygen measurement approach and are necessary for adopting this technique as a reliable pulmonary marker.

Measurements of Lung Ventilation Using Hyperpolarized Gases

Ventilation deficiencies are symptomatic of many obstructive and restrictive pulmonary diseases. Such abnormalities affect compliance and airway resistance and therefore change airflow and lung volume. These abnormalities in turn affect pulmonary ventilation, and therefore regional measurements of lung ventilation should be sensitive to these disease processes. Even with no additional means of contrast, important information can be learned by imaging a single breath of HP gas. Single-breath images can provide a qualitative picture of lung regions that may be improperly ventilated due to illnesses such as asthma or emphysema. As with chest X-rays or other qualitative radiologic methods, the single-breath image must be interpreted. However, with images of large signal-to-noise ratios and high spatial resolution, the interpretation can often be performed easily without radiologic training. Several researchers have therefore used single-breath HP gas images of lungs to assess the sensitivity of this modality for various pulmonary diseases such as asthma, emphysema, and cystic fibrosis.

The only technique currently implemented for quantitative assessment of lung ventilation during inhalation is based on the work of Deninger and coworkers (34). The regional fractional ventilation, commonly represented by r, is defined as the ratio of the volume of fresh gas added to an element of the lung during inspiration, V_f, to the total gas volume of that element at the end of inspiration, V_t (comprising V_f and the residual volume, V_r), $r = V_f/V_t$. Experimentally, fractional ventilation may be measured based on the increase in signal intensity due to the build-up of HPG in the lung over an increasing number of HPG breaths. Several improvements to the original approach have been proposed in two recent and independent studies (35, 36), to reduce the required volume of HPG and acquisition time to a range that can potentially make the implementation feasible in human subjects.

The fractional ventilation technique, however, only gives a steady-state measurement of gas distribution in the small airways. Due to the significance of gas flow dynamics in the pathophysiology of obstructive pulmonary diseases, especially during forced exhalation, several investigators have begun developing techniques for the dynamic imaging of gas flow in the lungs. In current clinical practice, the standard metric of pulmonary function derived from spirometry, the forced expiratory volume in one second (FEV_1), is used as the key criterion in classifying patients with COPD. It is believed that a regional metric for gas exhalation rate can provide a more sensitive tool to identify airway obstruction than global spriomteric measures, which have been shown to be insensitive to regional changes of lung function (37). Due to inherent challenges in dynamic imaging polarized gases, studies have mostly used qualitative or semi-quantitative methods for the measurement of regional ventilation in large animals and human subjects. In one study, investigators examined nine patients with mild/moderate to severe asthma and compared physiologic abnormalities obtained from dynamic images to results from standard spirometry, body plethysmography, and CT (38). Gas clearance from the lungs was quantified by comparing the SNR change between images acquired immediately before and after forced expiration. This highlighted the regions of differential gas clearance and trapping that were confirmed as such by CT imaging. The same group of researchers extended the dynamic imaging technique to 3D imaging of the whole lung with multiple half-echo radial trajectories that allow for imaging acceleration

through undersampling (39). This technique has made it possible to acquire 3D whole volume images of the lung at an isotropic resolution of 3.28 mm^3 and a temporal resolution of approximately 1 second.

Animal models of emphysema and asthma have been of interest to the HPG MRI community as platforms for developing ventilation techniques sensitive to airway obstruction. Among these models, the elastase-induced model of emphysema and the methacholine-induced bronchoconstriction model of asthma are popular due to their straightforward implementation and repeatable results. Emami and colleagues studied the early changes of lung function and structure in presence of an elastase-induced model of emphysema at mild and moderate severities in cohorts of rats (40). Regional fractional ventilation was measured in rat lungs by HP ^{3}He MRI at 5 and 10 weeks into the experiment. Lm was measured from histologic slices taken from the centers of each lobe and results were compared with lobar averages of fractional ventilation. The results indicated that the mean fractional ventilation was significantly different between healthy control subjects (0.23 ± 0.04) and emphysematous animals at both time points in the moderate group (0.06 ± 0.02 and 0.12 ± 0.05, respectively). However, changes in average alveolar diameter between healthy and emphysematous rats were not statistically observable until the tenth week. Moreover, analysis of the correlation between lung function and structure on a lobar basis suggested that the majority of the decline in fractional ventilation occurred in the first 5 weeks, while enlargement of alveolar diameters appeared primarily between the fifth and tenth weeks. In a different study, Driehuys and coworkers applied a radial acquisition scheme to study ventilation defects in an asthma model of mice before and after bronchoconstriction induced by methacholine (MCh) (41). Their work demonstrated the acquisition of 3D images of mouse airway structure at a resolution of $125 \times 125 \times 1{,}000$ μm^3, where diffusion becomes a hindrance to airway resolution. Images of ovalbumin-sensitized mice acquired after MCh showed both airway closure and ventilation loss.

Regarding the translation of ventilation imaging techniques to the diagnosis of human pulmonary diseases, de Lange and colleagues reported the most recent study on a group of subjects with asthma (42). The researchers for that study assessed and compared ventilation defects before and immediately after a MCh challenge in 10 young subjects with asthma on two different days using spirometry and HPG MRI. Comparison of the images from the two days revealed that around 41% of the pre-MCh defects and 69% of the post-MCh defects were in the same location, and of those, 69% of pre-MCh defects and 43% of post-MCh defects did not change in size. Comparing pre-MCh and post-MCh images, on the other hand, revealed that the percent increase in defects caused by MCh was much greater than the percent decrease in spirometric parameters, indicating a higher sensitivity of imaging metrics to the presence of ventilation defects.

Other researchers have looked at asymptomatic lung conditions that could play an important role in the proper diagnosis of ventilation defects in the otherwise healthy subjects. Parraga and coworkers reported ventilation defects that were reproducible in same-day scanning and 7-day scanning visits in elderly healthy volunteers (43). In a different study, Mata and colleagues investigated immobilization-induced ventilation defects when performing HPG MRI of the lung (44). Twelve healthy subjects underwent HP ^{3}He MRI of the lungs after inhalation of HPG at three time points: immediately after being positioned supine in the MRI scanner, after 45 minutes remaining supine, and immediately thereafter after having turned prone. The results indicated that immobilization of the subject for an extended period of time led to an increased number of ventilation defects in the dependent regions of the lung, and therefore suggested that any unnecessary delay in acquiring images after positioning the subject in the MRI scanner should be avoided.

As mentioned earlier, a measurement of lung ventilation is already available through the inhalation of a radioactive tracer and its detection with a γ-ray nuclear medicine scanner. Its use, however, is limited due to a low spatial and temporal resolution along with a necessitated exposure to ionizing radiation. The most common clinical applications for a ventilation scan are the detection of pulmonary emboli, both acute and chronic. It recently has largely been supplanted by the CT scan for the diagnosis of acute pulmonary emboli, but it is still the test of choice for chronic pulmonary emboli (45). Ventilation imaging with ^{3}He MRI has several advantages over its nuclear medicine counterpart, and therefore its potential clinical applications are broader. The most important difference is that techniques are being developed to not just show ventilation defects, but to quantify them. This would be akin to having very sensitive spirometry measurements on a regional basis. This functional assessment of ventilation could broaden areas of investigation to the diagnosis of previously elusive pathologies like small airways disease. There is currently no reliable way to accurately diagnose small airways disease. Pulmonary function tests are very insensitive, as are CT scans (46). CT scans also will not show structural changes until late in the disease, and therefore there is a reliance on more functional measurements like expiratory image gas trapping. The study of dynamic ventilation could revolutionize the way we diagnose and treat patients with small airways disease. One of the most obvious populations this would benefit is the post–lung transplant population, where long-term survival is hampered by the ubiquitous development of small airways disease after a period of several years; there are a broad range of patients afflicted with small airways diseases whose conditions take far too long to diagnose.

Preliminary validation of fractional ventilation techniques have been performed in phantoms (36) with *a priori* knowledge of the gas replacement ratio. Other researchers have used computational fluid dynamics (CFD) techniques to validate flow measurements with hyperpolarized gas MRI velocimetry in artificial models of human proximal airways. Using this approach, de Rochefort and coworkers performed a three-dimensional numerical validation of air flow in a model of a pulmonary system under steady inspiration and extracted velocity maps down to the fourth airway generation using ^{3}He MRI and the corresponding CFD model over a period of a few seconds (47). The experimental and simulation results agreed within a 3% margin of error. Main and secondary flow velocity intensities were also shown to be similar, as were velocity convective patterns. This approach, however, is only valid in the conductive airway region, where convection is the dominant transport mechanism. Validation of quantitative ^{3}He ventilation imaging at the acinar and alveolar level is the subject of ongoing research, and several approaches may be worth the exploration, such as the gold standard of inhaled microspheres in the form of aerosols that have been traditionally used to assess regional ventilation (48), as well as xenon-enhanced CT ventilation scans with an already demonstrated performance level (49).

Measurements of Lung Perfusion Using Hyperpolarized MRI

The regional measurements of oxygen tension and uptake can be used for *indirect* calculation of pulmonary perfusion. A technique developed by Rizi and colleagues permits the calculation of regional ventilation–perfusion ratios, ($\dot{V}_A/\dot{Q}$) from

measured $P_{A_{O_2}}$ on a regional basis (50). In the past, the investigators have used known values for $\dot{V}_A/\dot{Q}$, inspired oxygen fraction ($F_{I_{O_2}}$), mixed venous P_{O_2} ($P\bar{v}_{O_2}$), and mixed venous PCO_2 ($P\bar{v}_{CO_2}$) to calculate unknown alveolar gas tensions ($P_{A_{O_2}}$ and $P_{A_{CO_2}}$). However, in this technique, $\dot{V}_A/\dot{Q}$ is calculated from local Pa_{O_2}measurements. This so-called *inverse problem* employs well-established equations of steady-state exchange of O_2, CO_2, and N_2 to determine the local $\dot{V}_A/\dot{Q}$ ratio. Like the initial method, known as *forward problem*, the inverse problem begins with the steady-state mass balances for gas exchange, which results in four equations with four unknowns: $P_{A_{O_2}}$, $P_{A_{CO_2}}$, $\dot{V}_I/\dot{Q}$ (the ratio of inspired ventilation to local perfusion, Q), and P_AN_2. In the forward problem, these equations are reduced to two equations with two unknowns ($\dot{V}_A/\dot{Q}$ and $P_{A_{CO_2}}$), while in the inverse problem, the four equations are reduced to one equation with one unknown ($P_{A_{CO_2}}$). The resulting $P_{A_{CO_2}}$ is then inserted into one of the equations used in the forward problem to calculate $\dot{V}_A/\dot{Q}$ (50). Separate measurement of regional ventilation through other techniques then allows for calculating regional perfusion from the calculated $\dot{V}_A/\dot{Q}$ value.

Liquid phase hyperpolarized nuclei can potentially be used for the direct measurement of pulmonary perfusion. Ishii and coworkers demonstrated the use of an HP ^{13}C compound for acquiring lung perfusion maps in pig lungs (51). Images were obtained using a trueFISP pulse sequence at a temporal resolution of 0.47 seconds. Figure 3(a) shows the ^{13}C image series of the pig's abdomen and thorax, as the contrast agent flows through the inferior vena cava and into the pulmonary arteries before it is completely distributed throughout the lung parenchyma. By fitting the signal dynamics to a Kety-Schmidt–like model on a regional basis (corrected for RF depolarization and estimated T_1 relaxation), the normalized perfusion map of the lung was estimated as shown in Figure 3(b). The results show the potential for obtaining high spatial (2.5 mm planar) and temporal (better than 500 ms) resolution images of pulmonary perfusion using ^{13}C-based contrast agents.

CHALLENGES AND OPPORTUNITIES

The feasibility of hyperpolarized gas imaging was first demonstrated nearly 15 years ago. The potential for noninvasive, nonirradiative, quantitative measurements of lung structure and function were recognized immediately, and extensive technique development has led to a diverse suite of function- and structure-specific imaging methods. Each method yields information that is unique and difficult to obtain in any other way. Nonetheless, hyperpolarized nuclei MRI is not yet a clinical technique, nor is it commonly used as a standard metric of disease state and progression in drug development trials or other studies. Researchers and clinicians in this field face several challenges, which present unique opportunities for the future of advancement of this powerful imaging technology.

First, the technology has been perceived as expensive and difficult to operate. This perception is largely a result of the fact that the polarization apparatuses in use at most sites are located within complex facilities, which present problems of space requirements and organizational requirements for extensive manual interaction. Consequently, significant training is necessary to ensure a robust operation. In addition, nucleus-specific MR hardware components including broadband MR transmit and receive amplifiers and chest RF coils, not commonly available on conventional proton (^1H) MRI scanners in medical centers, plus complications associated with obtaining research agreements from the technology patent holder, have added to this complexity. Nevertheless, as potential clinical applications of multi-nucleus MRI techniques (such as ^{23}Na and ^{13}C) are expanding, many manufacturers have started providing broadband capabilities both to existing scanners and to new installations as a standard feature.

Second, the HP MRI community has not adequately established standard imaging techniques. This lack of establishment is particularly notable in ADC imaging, in which the chosen diffusion sensitizing parameters affect the resulting ADC values. Achieving consensus among research groups, and rigorously testing compatibility of results across clinical centers, are among the steps needed to encourage the adoption of standards that will give the field a foundation of easily replicated and validated techniques.

Recent developments in regards to the cost and supply of ^3He gas have rightfully raised concerns regarding long-term availability of this noble gas for medical imaging applications. It is, however, worth noting that almost all HP ^3He MRI techniques are directly translatable to HP ^{129}Xe as a means of overcoming the limited supply. With the advent of high capacity and continuous ^{129}Xe hyperpolarizing technology (52, 53), the

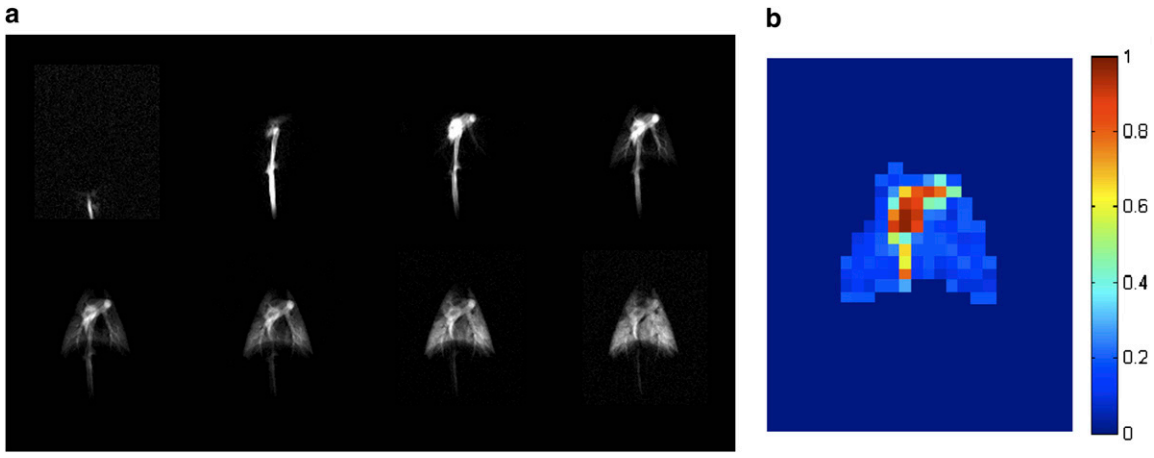

Figure 3. Sequential images of porcine lung perfusion after injection of 5 ml of 50mM hyperpolarized ^{13}C-labeled hydroxyethyl propionate at a rate of 1 ml/second (a) and the results of a regional fit to the quantitative tracer wash-in/-out model. Note that the results of the fit are meaningful only in the regions corresponding to lung vasculature and parenchyma, as the arterial input function is not appropriate for voxels in the heart and vena cava. Reprinted by permission from Reference 51.

elimination of the limit on the quantity of polarized gas available in one imaging session is getting closer to becoming a reality. The anesthetic properties of xenon, however, remain a challenge for implementation in humans. Human xenon inhalation is limited by anesthetic considerations to a less than 35% alveolar concentration (54). Therefore, depending on the available polarization, the concentration of the inhaled gas and the number of breaths should be optimally selected to limit the alveolar concentration of this gas while providing reasonable measurement accuracy.

Finally, no large-scale studies have been performed that unambiguously demonstrate the relative sensitivity and specificity advantages of the HPG MRI techniques. Although two published studies have shown convincingly that hyperpolarized gas-based methods are able to detect early changes in a smoker's lung that cannot be seen using any other measurement technique (12, 21), it is nonetheless possible that the changes measured do not correspond to early disease but instead are a relatively benign product of smoke exposure, such as chronic inflammation or increased mucus production. Hypotheses of this nature demand further investigation over a longer time period and with a larger sample size.

Conflict of Interest Statement: K.E. is half owner of an R&D-phase startup company that plans to manufacture hyperpolarization equipment. To date no sales have taken place. M.S. does not have a financial relationship with a commercial entity that has an interest in the subject of this manuscript. S.K. is half owner of an R&D-phase startup company that plans to sell hyperpolarization equipment. No sales have taken place to date. R.V.C. does not have a financial relationship with a commercial entity that has an interest in the subject of this manuscript. M.I. does not have a financial relationship with a commercial entity that has an interest in the subject of this manuscript. R.R.R. does not have a financial relationship with a commercial entity that has an interest in the subject of this manuscript.

References

1. Ball WC Jr, Stewart PB, Newsham LG, Bates DV. Regional pulmonary function studied with xenon 133. *J Clin Invest* 1962;41:519–531.
2. Coxson HO. Quantitative computed tomography assessment of airway wall dimensions: current status and potential applications for phenotyping chronic obstructive pulmonary disease. *Proc Am Thorac Soc* 2008;5:940–945.
3. Failo R, Wielopolski PA, Tiddens HA, Hop WC, Pozzi Mucelli R, Lequin MH. Lung morphology assessment using MRI: a robust ultrashort tr/te 2d steady state free precession sequence used in cystic fibrosis patients. *Magn Reson Med* 2009;61:299–306.
4. Fan L, Liu SY, Xiao XS, Sun F. Demonstration of pulmonary perfusion heterogeneity induced by gravity and lung inflation using arterial spin labeling. *Eur J Radiol* (In press)
5. Ohno Y, Iwasawa T, Seo JB, Koyama H, Takahashi H, Oh YM, Nishimura Y, Sugimura K. Oxygen-enhanced magnetic resonance imaging versus computed tomography: multicenter study for clinical stage classification of smoking-related chronic obstructive pulmonary disease. *Am J Respir Crit Care Med* 2008;177:1095–1102.
6. Happer W. Optical pumping. *Rev Mod Phys* 1972;44:169–249.
7. Walker TG, Happer W. Spin-exchange optical pumping of noble-gas nuclei. *Rev Mod Phys* 1997;69:629–642.
8. Chen XJ, Moller HE, Chawla MS, Cofer GP, Driehuys B, Hedlund LW, Johnson GA. Spatially resolved measurements of hyperpolarized gas properties in the lung in vivo. Part I: Diffusion coefficient. *Magn Reson Med* 1999;42:721–728.
9. Yablonskiy DA, Sukstanskii AL, Leawoods JC, Gierada DS, Bretthorst GL, Lefrak SS, Cooper JD, Conradi MS. Quantitative in vivo assessment of lung microstructure at the alveolar level with hyperpolarized 3He diffusion MRI. *Proc Natl Acad Sci USA* 2002;99:3111–3116.
10. Salerno M, Altes TA, Brookeman JR, de Lange EE, Mugler JP III. Rapid hyperpolarized 3He diffusion MRI of healthy and emphysematous human lungs using an optimized interleaved-spiral pulse sequence. *J Magn Reson Imaging* 2003;17:581–588.
11. Morbach AE, Gast KK, Schmiedeskamp J, Dahmen A, Herweling A, Heussel CP, Kauczor HU, Schreiber WG. Diffusion-weighted MRI of the lung with hyperpolarized helium-3: a study of reproducibility. *J Magn Reson Imaging* 2005;21:765–774.
12. Fain SB, Panth SR, Evans MD, Wentland AL, Holmes JH, Korosec FR, O'Brien MJ, Fountaine H, Grist TM. Early emphysematous changes in asymptomatic smokers: detection with 3He MR imaging. *Radiology* 2006;239:875–883.
13. Saam BT, Yablonskiy DA, Kodibagkar VD, Leawoods JC, Gierada DS, Cooper JD, Lefrak SS, Conradi MS. Mr imaging of diffusion of (3)He gas in healthy and diseased lungs. *Magn Reson Med* 2000;44:174–179.
14. Woods JC, Yablonskiy DA, Chino K, Tanoli TSK, Cooper JD, Conradi MS. Magnetization tagging decay to measure long-range ^{3}He diffusion in healthy and emphysematous canine lungs. *Magn Reson Med* 2004;51:1002–1008.
15. Dugas JP, Garbow JR, Kobayashi DK, Conradi MS. Hyperpolarized ^{3}He MRI of mouse lung. *Magn Reson Med* 2004;52:1310–1317.
16. Conradi MS, Yablonskiy DA, Woods JC, Gierada DS, Jacob RE, Chang YV, Choong CK, Sukstanskii AL, Tanoli T, Lefrak SS, *et al.* ^{3}He diffusion MRI of the lung. *Acad Radiol* 2005;12:1406–1413.
17. Woods JC, Yablonskiy DA, Choong CK, Chino K, Pierce JA, Hogg JC, Bentley J, Cooper JD, Conradi MS, Macklem PT. Long-range diffusion of hyperpolarized 3He in explanted normal and emphysematous human lungs via magnetization tagging. *J Appl Physiol* 2005; 99:1992–1997.
18. Wang C, Miller GW, Altes TA, de Lange EE, Cates GD Jr, Mugler JP III. Time dependence of 3He diffusion in the human lung: measurement in the long-time regime using stimulated echoes. *Magn Reson Med* 2006;56:296–309.
19. Fishman A, Martinez F, Naunheim K, Piantadosi S, Wise R, Ries A, Weinmann G, Wood DE. A randomized trial comparing lung-volume–reduction surgery with medical therapy for severe emphysema. *N Engl J Med* 2003;348:2059–2073.
20. Calverley PM, Anderson JA, Celli B, Ferguson GT, Jenkins C, Jones PW, Yates JC, Vestbo J. Salmeterol and fluticasone propionate and survival in chronic obstructive pulmonary disease. *N Engl J Med* 2007; 356:775–789.
21. Diaz S, Casselbrant I, Piitulainen E, Magnusson P, Peterson B, Wollmer P, Leander P, Ekberg O, Akeson P. Validity of apparent diffusion coefficient hyperpolarized (3)He-MRI using msct and pulmonary function tests as references. *Eur J Radiol* 2008;27:763–770.
22. Woods J, Choong C, Yablonskiy D, Bentley J, Wong J, Pierce J, Cooper J, Macklem P, Conradi M, Hogg J. Hyperpolarized 3He diffusion MRI and histology in pulmonary emphysema. *Magn Reson Med* 2006; 56:1293–1300.
23. Jacob RE, Minard KR, Laicher G, Timchalk C. 3D 3He diffusion MRI as a local in vivo morphometric tool to evaluate emphysematous rat lungs. *J Appl Physiol* 2008;105:1291–1300.
24. Saam B, Happer W, Middleton H. Nuclear relaxation of ^{3}He in the presence of O_2. *Phys Rev A* 1995;52:862–865.
25. Fischer MC, Spector ZZ, Ishii M, Yu J, Emami K, Itkin M, Rizi RR. Single-acquisition sequence for the measurement of oxygen partial pressure by hyperpolarized gas MRI. *Magn Reson Med* 2004;52:766–773.
26. Deninger AJ, Eberle B, Bermuth J, Escat B, Markstaller K, Schmiedeskamp J, Schreiber WG, Surkau R, Otten E, Kauczor HU. Assessment of a single-acquisition imaging sequence for oxygen-sensitive ^{3}He-MRI. *Magn Reson Med* 2002;47:105–114.
27. Fischer MC, Yu J, Ishii M, Spector ZZ, Emami K, Itkin M, Jalali A, Rizi RR. Single-acquisition sequence for the measurement of regional alveolar oxygen pressure and oxygen depletion rate by ^{3}He MRI. Proceedings of the 12th Annual Meeting of International Society for Magnetic Resonance in Medicine (ISMRM). Kyoto, Japan: Proceedings of the 12th Annual Meeting of International Society for Magnetic Resonance in Medicine (ISMRM); 2004.
28. Yu J, Ishii M, Law M, Woodburn JM, Emami K, Kadlecek S, Vahdat V, Guyer RA, Rizi RR. Optimization of scan parameters in pulmonary partial pressure oxygen measurement by hyperpolarized 3He MRI. *Magn Reson Med* 2008;59:124–131.
29. Yu J, Law M, Kadlecek S, Emami K, Ishii M, Woodburn JM, Vahdat V, Rizi RR. Simultaneous measurement of pulmonary partial pressure oxygen and apparent diffusion coefficient by hyperpolarized 3He MRI. *Magn Reson Med* (In press)
30. Yu J, Rajaei S, Ishii M, Law M, Emami K, Woodburn JM, Kadlecek S, Vahdat V, Rizi RR. Measurement of pulmonary partial pressure of oxygen and oxygen depletion rate with hyperpolarized helium-3 MRI: a preliminary reproducibility study on pig model. *Acad Radiol* 2008; 15:702–712.
31. Patz S, Hersman FW, Muradian I, Hrovat MI, Ruset IC, Ketel S, Jacobson F, Topulos GP, Hatabu H, Butler JP. Hyperpolarized

(129)Xe MRI: a viable functional lung imaging modality? *Eur J Radiol* 2007;64:335–344.
32. West JB. Respiratory physiology: the essentials. Philadelphia: Lippincott Williams & Wilkins; 2008.
33. Gast KK, Schreiber WG, Herweling A, Lehmann F, Erdos G, Schmiedeskamp J, Kauczor HU, Eberle B. Two-dimensional and three-dimensional oxygen mapping by 3He-MRI validation in a lung phantom. *Eur Radiol* 2005;15:1915–1922.
34. Deninger AJ, Mansson S, Petersson JS, Pettersson G, Magnusson P, Svensson J, Fridlund B, Hansson G, Erjefeldt I, Wollmer P, *et al.* Quantitative measurement of regional lung ventilation using ^{3}He MRI. *Magn Reson Med* 2002;48:223–232.
35. Santyr GE, Lam WW, Ouriadov A. Rapid and efficient mapping of regional ventilation in the rat lung using hyperpolarized 3He with flip angle variation for offset of rf and relaxation (FAVOR). *Magn Reson Med* 2008;59:1304–1310.
36. Emami K, Kadlecek S, Woodburn JM, Zhu J, Yu J, Vahdat V, Pickup S, Ishii M, Rizi RR. Improved technique for measurement of regional fractional ventilation by hyperpolarized 3He MRI. *Magn Reson Med* (In press)
37. Takasugi JE, Godwin JD. Radiology of chronic obstructive pulmonary disease. *Radiol Clin North Am* 1998;36:29–55.
38. Holmes JH, Korosec FR, Du J, O'Halloran RL, Sorkness RL, Grist TM, Kuhlman JE, Fain SB. Imaging of lung ventilation and respiratory dynamics in a single ventilation cycle using hyperpolarized He-3 MRI. *J Magn Reson Imaging* 2007;26:630–636.
39. Holmes JH, O'Halloran RL, Brodsky EK, Jung Y, Block WF, Fain SB. 3D hyperpolarized He-3 MRI of ventilation using a multi-echo projection acquisition. *Magn Reson Med* 2008;59:1062–1071.
40. Emami K, Cadman RV, Woodburn JM, Fischer MC, Kadlecek SJ, Zhu J, Pickup S, Guyer RA, Law M, Vahdat V, *et al.* Early changes of lung function and structure in an elastase model of emphysema: a hyperpolarized 3He MRI study. *J Appl Physiol* 2008;104:773–786.
41. Driehuys B, Walker J, Pollaro J, Cofer GP, Mistry N, Schwartz D, Johnson GA. 3He MRI in mouse models of asthma. *Magn Reson Med* 2007;58:893–900.
42. de Lange EE, Altes TA, Patrie JT, Parmar J, Brookeman JR, Mugler JP III, Platts-Mills TA. The variability of regional airflow obstruction within the lungs of patients with asthma: assessment with hyperpolarized helium-3 magnetic resonance imaging. *J Allergy Clin Immunol* 2007;119:1072–1078.
43. Parraga G, Mathew L, Etemad-Rezai R, McCormack DG, Santyr GE. Hyperpolarized 3He magnetic resonance imaging of ventilation defects in healthy elderly volunteers: initial findings at 3.0 tesla. *Acad Radiol* 2008;15:776–785.
44. Mata J, Altes T, Knake J, Mugler J III, Brookeman J, de Lange E. Hyperpolarized 3He MR imaging of the lung: effect of subject immobilization on the occurrence of ventilation defects. *Acad Radiol* 2008;15:260–264.
45. Tunariu N, Gibbs SJ, Win Z, Gin-Sing W, Graham A, Gishen P, Al-Nahhas A. Ventilation-perfusion scintigraphy is more sensitive than multidetector CTPA in detecting chronic thromboembolic pulmonary disease as a treatable cause of pulmonary hypertension. *J Nucl Med* 2007;48:680–684.
46. Ryu JH, Myers JL, Swensen SJ. Bronchiolar disorders. *Am J Respir Crit Care Med* 2003;168:1277–1292.
47. de Rochefort L, Vial L, Fodil R, Maitre X, Louis B, Isabey D, Caillibotte G, Thiriet M, Bittoun J, Durand E, *et al.* In vitro validation of computational fluid dynamic simulation in human proximal airways with hyperpolarized 3He magnetic resonance phase-contrast velocimetry. *J Appl Physiol* 2007;102:2012–2023.
48. Robertson HT, Hlastala MP. Microsphere maps of regional blood flow and regional ventilation. *J Appl Physiol* 2007;102:1265–1272.
49. Marcucci C, Nyhan D, Simon BA. Distribution of pulmonary ventilation using Xe-enhanced computed tomography in prone and supine dogs. *J Appl Physiol* 2001;90:421–430.
50. Rizi RR, Baumgardner JE, Ishii M, Spector ZZ, Edvinsson JM, Jalali A, Yu J, Itkin M, Lipson DA, Gefter W. Determination of regional $\dot{V}_A/\dot{Q}$ by hyperpolarized 3He MRI. *Magn Reson Med* 2004;52:65–72.
51. Ishii M, Emami K, Kadlecek S, Petersson JS, Golman K, Vahdat V, Yu J, Cadman RV, MacDuffie-Woodburn J, Stephen M, *et al.* Hyperpolarized ^{13}C MRI of the pulmonary vasculature and parenchyma. *Magn Reson Med* 2007;57:459–463.
52. Driehuys B, Pollaro J, Cofer GP. In vivo MRI using real-time production of hyperpolarized 129Xe. *Magn Reson Med* 2008;60:14–20.
53. Hersman FW, Ruset IC, Ketel S, Muradian I, Covrig SD, Distelbrink J, Porter W, Watt D, Ketel J, Brackett J, *et al.* Large production system for hyperpolarized 129Xe for human lung imaging studies. *Acad Radiol* 2008;15:683–692.
54. Patz S, Muradian I, Hrovat MI, Ruset IC, Topulos G, Covrig SD, Frederick E, Hatabu H, Hersman FW, Butler JP. Human pulmonary imaging and spectroscopy with hyperpolarized 129Xe at 0.2t. *Acad Radiol* 2008;15:713–727.